Applied Catalysis B: Environmental 203 (2017) 43–52

Contents lists available at ScienceDirect

Applied Catalysis B: Environmental

journal homepage: www.elsevier.com/locate/apcatb

Solar-irradiation driven biodiesel production using Cr/SiO_2 photocatalyst exploiting cooperative interaction between Cr^{6+} and Cr^{3+} moieties

Grisel Corro [a,*], Nallely Sánchez [a], Umapada Pal [b], Surinam Cebada [a], José Luis García Fierro [c]

[a] Instituto de Ciencias, Benemerita Universidad Autonoma de Puebla, 4 sur 104, 72000 Puebla, Mexico
[b] Instituto de Fisica, Benemerita Universidad Autonoma de Puebla, Apdo, Postal J-48, 72570 Puebla, Mexico
[c] Instituto de Catálisis y Petroleoquímica, Cantoblanco, 28049 Madrid, Spain

ARTICLE INFO

Article history:
Received 14 May 2016
Received in revised form
26 September 2016
Accepted 3 October 2016
Available online 4 October 2016

Keywords:
Biodiesel
Photocatalytic esterification
Waste frying oil
Cr/SiO_2

ABSTRACT

The production of biodiesel from waste frying oil (WFO) by a two-step process was investigated. In the first step, the free fatty acids (FFAs) present in the oil were esterified with methanol by a photocatalytic process using Cr/SiO_2 semiconductor composite and solar irradiation as light source. The catalytic performances of Cr/SiO_2 calcined at different temperatures (500–1000 °C) were investigated in FFAs photo-esterification process. The samples were characterized by X-ray diffraction (XRD), X-ray photoelectron spectroscopy, diffuse reflectance spectroscopy (DRS), and nitrogen physisorption. Characterization results revealed the presence of Cr^{6+} in the samples calcined at temperatures between 500 and 600 °C. However, a mixture of Cr^{6+} and Cr^{3+} was detected in the samples calcined at higher temperatures (700–1000 °C). The catalysts calcined between 700 and 1000 °C showed a very high activity for FFAs photo-esterification. A mechanism is proposed to explain this high photoactivity, assuming a synergetic electronic interaction between Cr^{6+} and Cr^{3+} during photo-irradiation, which generates H^+, $CH_3O^\bullet$ and $R{-}COOH^\bullet$ radicals in high concentration at the photocatalyst surface.

The second step consisted in the triglycerides transesterification with methanol through thermal activation using solar irradiation as heating source and catalyzed by NaOH. Produced biodiesel by this process, fulfills all the international requirements for its utilization as a fuel.

1. Introduction

The limited availability of conventional fossil fuels for internal combustion engines, associated effects of global warming, and other environmental issues arising from the combustion of fossil fuels are the most threatening problems to the modern civilization. Diesel engine is the most fuel-efficient combustion engine among the available ones. Use of diesel (a fossil fuel) engine in the transport sector is mainly due to its better fuel economy and efficient power conversion. On the other hand, biodiesel is the fastest growing alternative fuel, as it can be used in diesel engines without any modification of engine geometry. Several countries such as USA, Germany, France, Italy, Brazil, and Indonesia are using biodiesel blended with diesel [1].

Biodiesels are produced from feedstocks which are renewable in nature. Among the common feedstocks used for biodiesel production, 28% is soybean oil, 22% is palm oil, 20% is animal fats, 11% is coconut oil; while rapeseed, sunflower and olive oil are 5% each [2,3]. These feedstock oils are mostly edible. The use of edible oil as biodiesel feedstock competes with their human consumptions for food. Moreover, use of refined edible oils in biodiesel production has been estimated to account for 70% of the total production cost.

To address these concerns, researchers have been looking for alternative feedstocks, especially from non-edible plants, microbial sources and waste oils. Problems associated with these types of feedstocks are the presence of significant amount of impurities such as free fatty acids (FFAs), moisture, waxes and gums, which require additional processing steps before their usage for biodiesel production through the conventional base-catalyzed process.

* Corresponding author.
E-mail addresses: griselda.corro@correo.buap.mx (G. Corro), upal@ifuap.buap.mx (U. Pal), jlgfierro@icp.csis.es (J.L.G. Fierro).

http://dx.doi.org/10.1016/j.apcatb.2016.10.005
0926-3373/

Recently [4] we applied a combined two-step catalytic process similar to the processes proposed by Wang et al. [5] and Sharma et al. [6] for producing biodiesel from non-edible Jatropha curcas crude oil (JCCO) with high content of free fatty acids (FFAs), and the production of biodiesel from highly acidic waste frying oil. The FFAs present in JCCO were first esterified with methanol by a novel photocatalytic process under UV irradiation using ZnO/SiO_2 as the heterogeneous photocatalyst. The transesterification step was catalyzed by NaOH through thermal activation process. However, even though ZnO/SiO_2 presented a very high FFAs photo-esterification activity, it was ineffective under visible (solar) light. The photoreaction was performed using UV lamps in a sophisticate reactor that resulted in an increase in biodiesel production cost.

To overcome these problems, in this investigation, we prepared Cr/SiO_2 composite photocatalysts, which are of semiconducting nature, presenting strong photo-absorption both in the UV and visible electromagnetic regions (230, 380, 440 nm and between 500 and 700 nm), suggesting their utilization for the photocatalytic esterification of FFAs with methanol under solar irradiation. Waste frying oil with high FFA content has been utilized to investigate the activity of the photocatalysts in the photocatalytic esterification of FFAs.

2. Materials and methods

2.1. Waste frying oil

The waste frying oil (WFO) used for biodiesel production was a mixture of different vegetable oils, provided by local restaurants. The collected WFO was filtered and stored in a hermetically sealed PVC can for its composition analysis and utilization in biodiesel production. The analysis of chemical composition of the FFAs present in the oil was performed with a gas chromatograph–mass spectrometer HP 6890, provided with a 5973 Network Agilent Technologies detector. The employed standard method in the analysis of the FFAs was the NMX-F-017-SCFI-2005. The method consists in a direct injection of the sample in the HP5 column and further identification of the FFAs using a free fatty acids mixture provided by Sigma Aldrich.

2.2. Laboratory reactors

The FFAs photocatalytic esterification was performed in a photoreactor newly designed and built in our laboratory. The detail schematic drawing of the experimental set-up is shown in Fig. 1(A).

The reactor consisted of a sealed quartz container, fitted with a k-type thermocouple to monitor the reaction temperature. An average temperature of 35 °C was recorded by exposing the reactor to direct sunlight for 4 h. The average intensity of the solar irradiation striking into the reactor was measured inside the empty container with a Mac Solar irradiation detector. The intensities of the solar radiation for the wavelength range 254–320 nm (maximum at 280 nm), 260–360 nm (maximum at 310 nm), and 300–400 nm (maximum at 360 nm) were measured with an UVP irradiancemeter. Temperature rise of the reaction mixture was prevented by utilizing two simple electrical fans in order to avoid any thermal activation of the esterification photo-reaction. The container was provided with an internal magnetic stirrer for vigorous stirring of the reaction mixture, assuring a homogeneous irradiation of the reaction mixture. The power required by the magnetic stirrer and the fans was provided by a photovoltaic cell.

The transesterification of triglycerides was performed using a similar sealed quartz container fitted with a k-type thermocouple to monitor the reaction temperature and a magnetic stirrer for agitation (Fig. 1(B)). The container was placed inside a closed transparent cubic heating chamber ($50 \times 50 \times 50\ cm^3$) with glass windows, which collects heat directly from solar radiation and prevents its transfer from the reactor through convection. Temperatures between 60 and 65 °C were attained in the reaction mixture by adjusting the exposed area of the top surface of the heating chamber.

2.3. Catalysts

2.3.1. Catalysts preparation

Fumed SiO_2 (Aldrich 99.99%) powders were impregnated with appropriate amount of aqueous $Cr(NO_3)_3$ solution to obtain 1 wt% Cr over SiO_2. The suspension was stirred at room temperature for 1 h. After drying at 120 °C overnight, the catalyst was calcined in air at 500 °C for 4 h. The catalyst was designated as $Cr/SiO_2(500)$. Five more catalysts were prepared in the same way, calcinating at higher temperatures (600–1000 °C). The prepared catalysts were designated as $Cr/SiO_2(x)$, (x = 600, 700, 800, 900, and 1000 °C). For reference, $SiO_2(x)$ samples were prepared in the same way, without impregnating $Cr(NO_3)_3$ solution.

2.3.2. Catalysts characterization

Adsorption measurements were performed in a Belsorp Mini II (BEL, Japan) sorptometer. Total surface areas (S_g) were estimated by N_2 physisorption at 77 K using BET analysis methods. The sam-

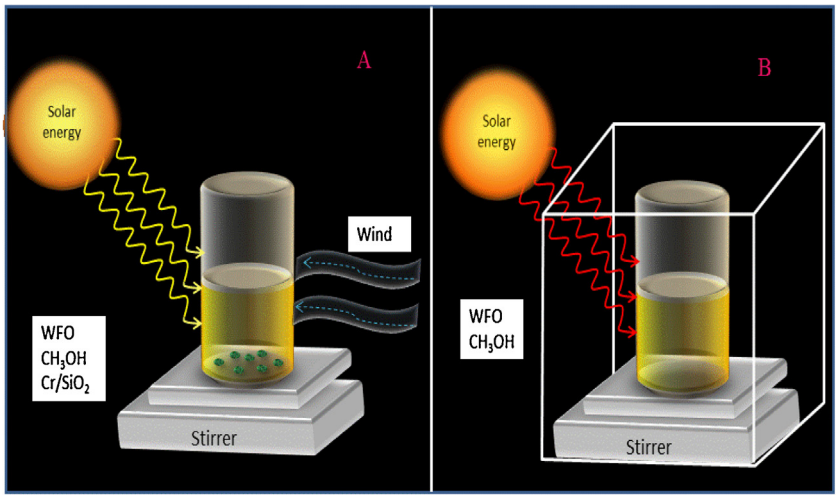

Fig. 1. Experimental set-up for (A) FFAs esterification, photocatalyzed by Cr/SiO_2 and (B) trliglycerides thermo-transesterification.

ples (0.5 g each) were degassed at 250 °C for 8 h before recording their physisorption isotherms. After cooling to room temperature, the isotherms were performed at a pressure range of 0–6.6 kPa. The technique of back extrapolation of the linear portion of the isotherms to zero equilibrium pressure was used to determine the saturation uptake.

Diffuse reflectance spectra (DRS) of the composite catalysts were obtained for the dry-pressed disk (~5 mm diameter) samples using a Shimadzu 2450 UV–vis spectrophotometer with a diffuse reflectance accessory, and $BaSO_4$ as standard reflectance sample.

X-ray photoelectron spectra (XPS) were recorded on freshly prepared $Cr/SiO_2(x)$ catalysts, using an Escalab 200R electron spectrometer equipped with a hemispherical analyzer, operating in a constant pass energy mode. Monochromatic MgK_α emission ($h\nu$ = 1253.6 eV) from the X-ray tube operating at 10 mA and 12 kV was utilized for recording the XPS spectra of the samples. Different energy regions of interest of the photoelectrons were scanned a number of times in order to get good signal-to-noise ratios. The intensities of the emission peaks were estimated by determining the integral of each peak after subtracting an S-shaped background and fitting the experimental peak to Lorentzian/Gaussian curves (80%L/20%G). The peak positions of the elements were corrected utilizing the position of *C1s* peak coming from adventitious carbon appeared at 284.9 ± 0.2 eV. High resolution XPS scan measurements for Cr2p regions were performed for each sample within 10 min in order to prevent possible photo-reduction of surface chromate species induced by X-ray irradiation during the measurement [7].

The crystallinity and structural phase of the obtained samples were verified through powder X-ray diffraction (XRD) technique using the CuKα source (λ = 1.5406 Å) of a Bruker D8 Discover diffractometer.

The specific acid and basic site density (number of acid- and basic-sites/g catalyst) at the catalyst surface were determined using a pH electrode (of 0–14 range, precision of 0.01, and temperature range of 0–100 °C). The basic site specific-density was determined according to the following process:

- The electrode was introduced in 20 ml of 0.05 M CH_3COOH standard solution, until no pOH variations were observed (pOH = 11).
- 1 g of fresh catalyst sample was added and the pOH evolution as a function of time was monitored until the neutralization equilibrium was observed.

The basic site specific-density of the catalyst was determined by calculating the $[OH^-]$ from the pOH equilibrium value.

The acid site specific-density was determined following the steps:

- The electrode was introduced in 20 ml of 0.05 M NaOH standard solution, until no pH variations were observed (pH = 12).
- 1 g of fresh catalyst sample was added and the pH evolution as a function of time was monitored until the neutralization equilibrium was observed.

The acid site specific-density of the catalyst was determined calculating $[H^+]$ from the pH equilibrium value.

2.4. Process for biodiesel production from WFO

The chemical processes proposed for the production of biodiesel are presented in Fig. 2. In the first step (Reaction 1), FFAs contained in the WFO were esterified with methanol using $Cr/SiO_2(x)$ photocatalysts and solar radiation as light source, at 35 °C. At the second step (Reaction (2)), sodium hydroxide was added to catalyze the

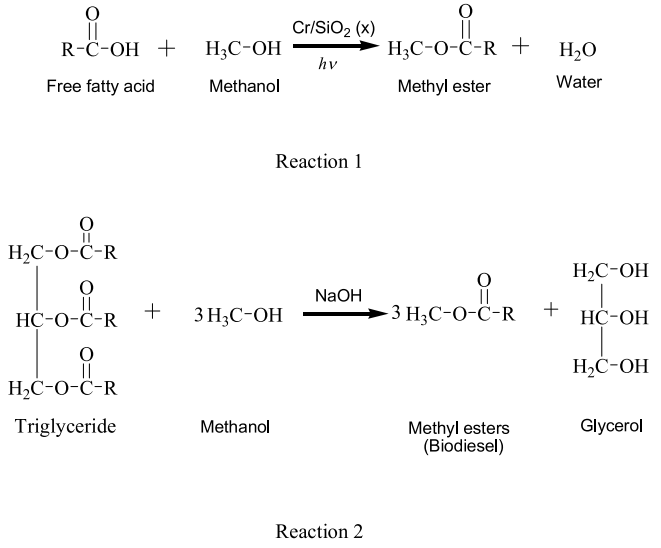

Fig. 2. Reaction mechanism of biodiesel synthesis by two-step catalytic process.

transesterification reaction, in which, the triglycerides react with methanol at 65 °C to produce methyl esters (biodiesel) and glycerol.

2.4.1. First step: FFAs photoesterification with methanol

2.4.1.1. Reaction conditions. The FFAs photoesterification experiments were performed at 35 °C in the reactor described in Fig. 1 (A). The reactants were methanol (Aldrich, 99%) and WFO. The methanol/WFO molar ratio was 12/1, according to the optimum value determined in our previous investigation [4]. The catalyst concentration was 7.5 wt% of the initial WFO mass. The speed of stirring was 400 rpm. The photocatalytic FFAs esterification was carried out under solar irradiation, exposing the reaction mixture during 11:00–15:00 h of the day, when the intensity of solar radiance was 1000–1200 kW/m^2. Four hours of solar irradiation was maintained for all the photoesterification experiments. In order to measure the effect of the solar irradiation on the FFA photoesterification activity of $Cr/SiO_2(x)$, the reactions were also performed at the same conditions in a dark box. The reaction temperature (35 °C) was attained using a laboratory electrical hot plate.

After 4 h of reaction, the mixture was left to settle to separate into two layers. The lower oily layer was composed of methyl esters produced by the FFAs photo-esterification. The unreacted triglycerides (which were further subjected to the transesterification reaction), and the solid, insoluble photocatalyst were recovered for further use. The upper layer was a mixture of methanol and water produced during Reaction (1) (Fig. 2).

The stability test of the $1\%Cr/SiO_2(1000)$ catalyst was performed by repeating the photo-esterification reaction 10 times with the same sample. The catalyst concentration was 1 wt% of the initial WFO mass, the speed of stirring was 400 rpm, the time of solar irradiation was 1 h. Under these conditions, only about 15% conversion of the FFA could be achieved. The stability study was conducted at low FFA conversion using a low catalyst concentration to prevent an excess of catalyst which might result in a non-apparent deactivation and a conversion which would still be high. Catalyst separated from the previous reaction mixture was used for the next run, without further washing or any other pretreatment.

2.4.1.2. Acid number determination. The acid numbers of the initial WFO and after its use in FFAs esterification were determined following the ASTM D 664 international standard method. This method consists in dissolving a test sample in a mixture of diethyl ether and ethanol and a further titration with a KOH solution. The

end-point was determined with a pH-meter equipped with glass and calomel electrodes.

The acid value A was determined using Eq. (1):

$$A = \frac{56.1 \times V \times c}{m} \quad (1)$$

where:

V = volume, in milliliters of standard volumetric potassium hydroxide solution used,

c = concentration, in moles per liter, of the standard volumetric potassium hydroxide solution used,

m = mass, in grams of the test portion

56.1 = molecular mass of potassium hydroxide.

2.4.1.3. Determination of % conversion of FFAs. The conversion of FFAs was defined as the fraction of FFAs that reacted during the esterification reaction with methanol. The % conversion of FFAs ($\%C_{FFA}$) was determined from the acid number ratio using the equation:

$$\%C_{FFA} = \frac{A_i - A_f}{A_i} \times 100, \quad (2)$$

where A_i is the initial acid number of the WFO and A_f is the final acid number of WFO after the FFAs esterification reaction.

2.4.2. Second step: alkali catalyzed transesterification of WFO

2.4.2.1. Reaction conditions. The mixture of the photo-esterified FFAs and the unreacted triglycerides was dried under stirring at 110 °C for 2 h, and transferred to a hermetic quartz reactor, similar to the one used for photoesterification process. The estimated water content was 0.158% as determined by Karl Fisher method (ISO 12937 Standard) [8]. Six times the stoichiometric amount of methanol required for total conversion of triglyceride and 1.0 wt% of NaOH were added as proposed by Zhang et al. [9]. Transesterification reactions of triglycerides with methanol were performed at 65 °C using solar heat for 30 min under stirring at 400 rpm. The mixture was left overnight to settle and separate in two layers. The upper layer was the fatty acid methyl esters (FAME) and the lower layer was the mixture of methanol, water and glycerol as indicated in reaction 2 (Fig. 1). The obtained FAME was washed with hot water (70 °C), and dried under stirring at 100 °C for 2 h, using an electrical heater operated by solar panel.

2.4.2.2. Chemical analysis of the produced biodiesel. The fatty acid methyl esters (FAME) content in the obtained biodiesel was estimated through gas chromatography (GC) analysis according to the EN 14103 test method. This test was performed to verify that the ester content in the obtained biodiesel was greater than 90% (m/m). On the other hand, the method permits a qualitative determination of the methyl esters composing the FAME. A methyl heptadecanoate solution was added to the biodiesel sample prior to its GC analysis. FAME content in the biodiesel was estimated using the relation:

$$FAME\ \% = \frac{\Sigma A - A_s}{A_s} \times \frac{C_s V_s}{m} \times 100, \quad (3)$$

where ΣA is the sum of signal areas of fatty acid methyl esters (C14:0-C24:1), A_s is the signal area of methyl heptadecanoate, C_s is the concentration of methyl heptadecanoate, V_s is the volume of standard solution, and m is the amount (mass) of biodiesel sample.

The linolenic acid methyl ester content L in the produced biodiesel was calculated using the relation:

$$L = \frac{A_L}{\left(\sum A\right) - A_{EI}} \times 100\%, \quad (4)$$

where $\sum A$ is the total signal area corresponding to the FAME (C14:0-C24:1), A_{EI} is the signal area of methylheptadecanoate, and A_L is the peak area of linolenic acid methyl ester.

The determination of the free, bound, total glycerin, and mono-, di-, and triglycerides, was performed according to the ASTM D 6584 test method, using the EZStart chromatography software provided by Shimadzu Co. The sample was analyzed after silyating with *N*-methyl-*N*-trimethylsilyltrifluoracetamide. For calibration, two internal standards and four reference materials were utilized. The contents of mono-, di-, and triglycerides were determined by comparing with monoolein, diolein, and triolein standards, respectively. Average conversion factors were applied to the mono-, di-, and triglycerides to calculate the bonded glycerin content in the sample.

2.4.2.3. Analysis of chromium traces in the produced biodiesel. The biodiesel obtained by the proposed process, in which the free fatty acids pre-esterification is performed using 1%Cr/SiO_2, could contain traces of chromium species. The presence of chromium species was determined following the UOP 391-09 test method, using a Shimadzu AA-7000 atomic absorption spectrophotometer, with a hollow Cr cathode lamp and a deuterium background corrector at respective wavelengths using an air-acetylene flame. The lamp current was set at 10 mA. Measurements were performed in the integrated absorbance mode at 357.9 nm, using a slit width of 0.5 nm. The biodiesel sample was dissolved in HNO_3 solution and kept in dark conditions for 2 weeks before the analysis.

3. Results and discussion

Estimated average intensity of the solar radiation inside the reactor exposed to sunlight was about 625 W/m^2. The intensities of UV radiations in different wavelength ranges inside the empty container are listed in Table 1.

3.1. WFO analysis

The composition of FFA determined by chemical analysis of WFO through GCMS is presented in Table 2. As can be seen, the WFO used in this study contains 11.69% FFAs.

3.2. Catalysts characterization

The evolution of the specific surface area of the Cr/SiO_2(x) and SiO_2(x) catalysts determined from their N_2 adsorption isotherms as a function of calcination temperature is presented in Fig. 3. The figure shows a similar evolution of specific surface area for the SiO_2(x) and Cr/SiO_2(x) catalysts with calcination temperature. The results

Table 1
Intensities of solar irradiation in different wavelength ranges inside the reactor container.

Wavelength range(nm)	Intensity (μW/m^2)
254–320	41
260–360	52
300–400	70

Table 2
FFAs content in the used WFO.

Compound	Content (%)
n-Hexadecanoic acid	8.42
Tetradecanedioic acid	3.27
Total FFAs content	11.69

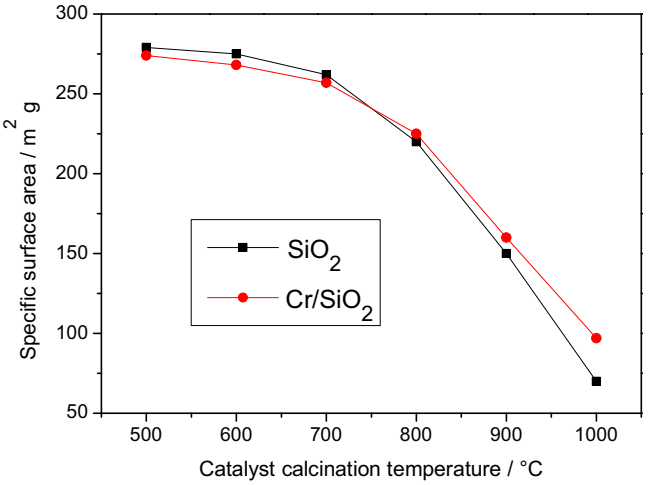

Fig. 3. Evolution of specific surface area of the catalysts as a function of their calcination temperature.

suggest that the presence of Cr in the SiO_2 does not affect much its crystallinity, size or porosity.

The acid and basic site specific densities in the catalysts are listed in Table 3. It can be seen that the SiO_2(x) samples present similar values of acid and basic site specific densities. The values vary only marginally with calcination temperature. Table 3 also shows that all the Cr/SiO_2(x) catalysts present only acid sites. Absence of basic sites in these catalysts might be due to the deposition of $Cr^{\delta+}$ species over SiO_2(x), covering the Lewis basic sites of SiO_2 surface during Cr impregnation. The presence of $Cr^{\delta+}$ species might have increased the Lewis acidity at the SiO_2 surface. Very high values of acid site specific density were measured for Cr/SiO_2(500), and Cr/SiO_2(600) samples. The value of acid site specific density decreased by two orders for Cr/SiO_2(700). A further increase of calcination temperature reduces the acid site specific density in Cr/SiO_2 dramatically. Apparently, the decrease of acid site specific density for calcinations between 700 and 800 °C is due to the thermal sintering of the catalyst, which decreases its specific surface area, consequently decreasing the acid site specific density. However, as can be seen in Table 3 and Fig. 3, while the variations of specific surface areas of Cr/SiO_2(x) and SiO_2(x) with calcination temperature (500–1000 °C) are very similar, the acid site specific density of SiO_2(x) varied only slightly with the decrease in specific surface area, and the same decreased drastically for Cr/SiO_2 for calcination temperatures 700 and 800 °C.

The drastic decrease in acid site specific density for the catalysts Cr/SiO_2(700) and Cr/SiO_2(800) can only be explained considering a reduction of Cr^{6+} species present at catalyst surface to form Cr^{3+} at these temperatures, resulting in a strong decrease of the surface Lewis acidity. The optical absorption spectra of the catalysts measured in the UV–vis spectral range presented in the following section fully support this assumption.

Table 3
Catalysts characterization data.

Catalyst (calcination temperature in °C)	Acid site specific density (sites/g catalyst)	Basic site specific density (sites/g catalyst)
SiO_2 (500)	9.55×10^{12}	1.25×10^{10}
SiO_2 (600)	7.62×10^{12}	2.29×10^{10}
SiO_2 (700)	5.97×10^{12}	4.57×10^{10}
SiO_2 (800)	5.22×10^{12}	7.81×10^{10}
SiO_2 (900)	3.17×10^{12}	1.60×10^{11}
SiO_2 (1000)	4.8×10^{11}	1.41×10^{11}
Cr/SiO_2 (500)	6.02×10^{19}	0
Cr/SiO_2 (600)	4.31×10^{19}	0
Cr/SiO_2 (700)	2.72×10^{17}	0
Cr/SiO_2 (800)	5.83×10^{13}	0
Cr/SiO_2 (900)	1.58×10^{13}	0
Cr/SiO_2 (1000)	1.34×10^{12}	0

Fig. 4 shows the optical absorption spectra of Cr/SiO_2(x) photocatalysts measured in diffuse reflectance mode in the UV–vis spectral range. The absorption spectra of Cr/SiO_2(500) and Cr/SiO_2(600) are dominated by two intense bands around 270 nm and 350 nm, a shoulder around 440 nm, and a weak band around 600 nm. The absorption bands centered on 270 and 350 nm are usually assigned to the transitions associated to charge transfer from O^{2-} to Cr^{6+} of the tetrahedrally coordinated Cr^{6+} and indicate the presence of highly isolated Cr^{6+} ions inside the silica matrix [10–13]. The shoulder around 440 nm is characteristic of Cr^{6+} polychromate (—Cr—O—Cr—)n in the framework. Additionally, the weak peak around 600 nm evidences the presence of octahedral Cr^{3+} associated with the presence of extra framework Cr_2O_3 clusters. The absorption spectra of Cr/SiO_2(700), Cr/SiO_2(800), Cr/SiO_2(900), and Cr/SiO_2(1000) revealed signals of lower intensities around 270, 350, and 440 nm, indicating a decrease in the concentration of Cr^{6+} species. However, these spectra revealed a very strong absorption band spanning 550–750 nm, corresponding to the octahedral Cr^{3+} species in the catalyst [14]. The results indicate that during catalyst calcination at temperatures ≥ 700 °C, the concentration of the Cr_2O_3 species increases in expense of tetrahedrally coordinated Cr-oxide moieties.

In order to confirm the results revealed by the UV–vis spectra on the evolution of electronic state of Cr species at the catalyst surface with calcination temperature, XPS analysis was performed on 1%Cr/SiO_2(600) and 1%Cr/SiO_2(1000) catalysts. The Cr 2p emissions of 1%Cr/SiO_2(600) and 1%Cr/SiO_2(1000) are shown in Fig. 5. Corresponding binding energy (BE) values of Cr $2p_{3/2}$ level and the estimated atomic percentages of Cr species in different oxidation states are presented in Table 4. The XPS spectrum of 1%Cr/SiO_2(600) revealed Cr $2p_{3/2}$ emission band with two components located around 580.4 and 576.5 eV, corresponding to Cr^{6+} and Cr^{3+} states, respectively (Fig. 5) [7,15–18]. The photocatalyst 1%Cr/SiO_2(1000) revealed similar two-fold Cr $2p_{3/2}$ emission. However, the position of the component corresponding to Cr^{6+} is shifted to higher BE (581.6 eV). This BE increase may be due to dihydroxylation of hydroxyl groups over SiO_2 and an increase of the surface tension of the siloxane groups of the support induced at high temperature [17,18]. On the other hand, the content of chromium in Cr^{3+} state increased and the content of chromium in Cr^{6+} state decreased with

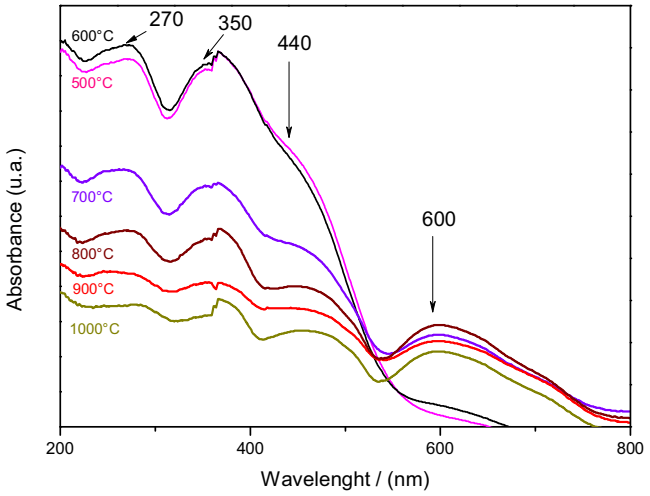

Fig. 4. UV–vis absorption spectra of Cr/SiO_2(x) photocatalysts (x = 500, 600, 700, 800, 900, and 1000).

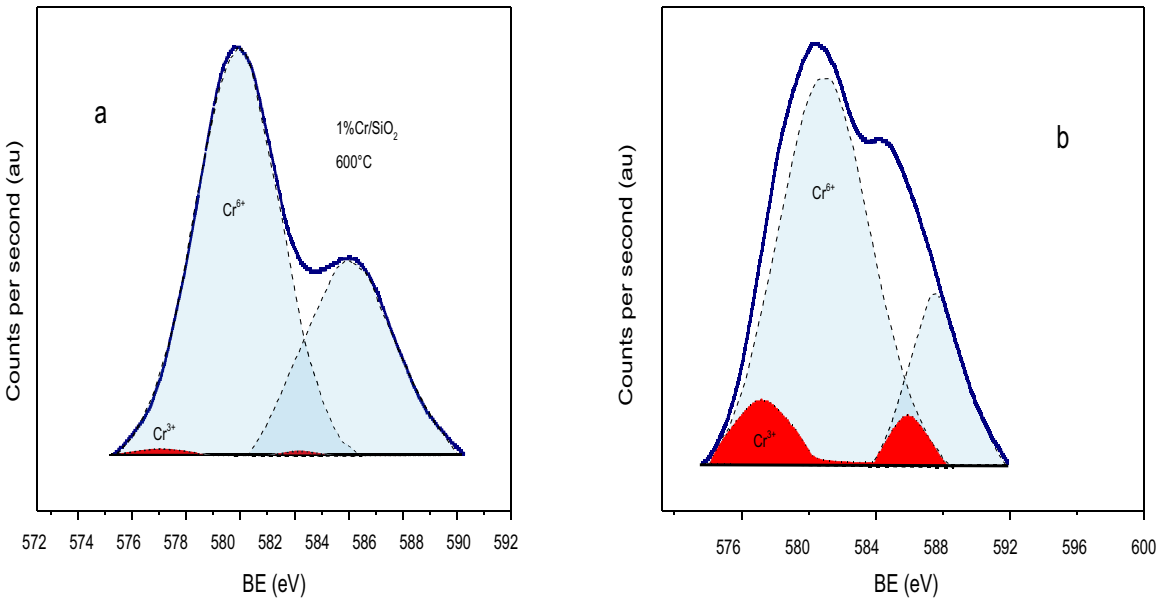

Fig. 5. XPS spectra of (a) 1% Cr/SiO_2(600) and (b) 1% Cr/SiO_2(1000).

Table 4
Binding energy positions of the components and atomic percentage at the surface of the 1%Cr/SiO_2 catalysts calcined at 600 °C and 1000 °C.

Catalyst	O*1s* (eV)	Cr $2p_{3/2}$ (eV)	Cr oxidation state assignment	Atomic percentage (%)
1%Cr/SiO_2(600)	532.8	580.4	Cr^{6+}	94.1
		576.5	Cr^{3+}	5.9
1%Cr/SiO_2(1000)	532.8	581.6	Cr^{6+}	82.4
		576.4	Cr^{3+}	17.6

the increase in calcination temperature of the catalysts. The results indicate that during calcination at 1000 °C a fraction of chromium in Cr^{6+} state transformed to surface stabilized trivalent Cr^{3+} state (Table 4).

The XPS spectra of 1%Cr/SiO_2(600) and 1%Cr/SiO_2(1000) are in agreement with the UV–vis absorption spectra results, which revealed a similar evolution of Cr^{6+} and Cr^{3+} states with calcination temperature. These results suggest that UV–vis spectroscopic analysis can be a useful and easy tool for determining the electronic state of chromium in Cr/SiO_2 catalysts, preventing the use of XPS analysis which is, in general, less available for continuous tests.

As can be seen from the XRD patterns of Cr/SiO_2(x) photocatalysts (Fig. 6), the samples Cr/SiO_2(700), Cr/SiO_2(800), Cr/SiO_2(900), and Cr/SiO_2(1000) (Fig. 6b) reveal weak reflections at 2θ of 24.6°, 33.6°, 36.2°, 41.7°, 44.6°, 50.3°, and 54.9°, characteristic of α-Cr_2O_3 phase [19–21]. However, the spectra of the Cr/SiO_2(500), and Cr/SiO_2(600) samples (Fig. 6a) revealed only the reflections of the support, with no reflection that can be assignable to chromium oxide phases, indicating that either chromium is highly dispersed in the catalyst or the size of Cr_xO_y nanoparticles are too small to be detected by XRD spectroscopy.

3.3. FFA photoesterification over Cr/SiO_2 catalysts

A possible general mechanism of the photocatalytic reactions through the generation of electron-hole pair and its function is as follows. On illuminating a semiconductor based heterogeneous photocatalyst by photons of energy higher than its band gap energy, electron-hole pairs are generated; which diffuse to the surface of the photocatalyst, initiating chemical reactions with the surrounding molecules. The free electrons (e^-) and holes (h^+) transform the surrounding molecules into free radicals [22]. During FFAs photoesterification under solar irradiation, the surrounding molecules are the methanol and FFAs present in the WFO.

Recent studies on hydrogen production through photocatalytic processes [23,24] indicate that methanol reacts with a positive hole, generating $CH_3O\cdot$ radicals during photocatalyst irradiation. On the other hand, the free electrons (e^-) generated over Cr/SiO_2 catalysts under solar irradiation react with FFAs present in WFO, as has been observed for the photolytic esterification of carboxylic acids with alcohols [25]. The possibilities of $CH_3O\cdot$ radical generation by the photogenerated holes (h^+) and the reaction between FFAs and the photogenerated free electrons (e^-) suggest that FFA esterification with methanol can be performed under solar irradiation in the presence of Cr/SiO_2(x) photocatalysts.

To determine the optimum calcination temperature of the catalysts for FFAs photoesterification reaction, we examined the photoactivity of all the samples calcined at different temperatures keeping the methanol/WFO mass ratio fixed at 12/1. The chosen particular methanol/WFO mass ratio was based on the optimum values determined in our previous study of the esterification of the FFA in Jatropha Curcas crude oil [4]. The catalyst/WFO mass ratio was fixed at 7.5/100 and the reaction temperature was kept at 35 °C. In absence of any photocatalyst, very low FFA% conversion was detected for the methanol/WFO mixture, even after 4 h of solar irradiation at 35 °C. The result indicates that the homogeneous photoesterification of FFA with methanol does not take place.

3.4. SiO_2(x) samples

First, we investigated the photoactivity of SiO_2(x) for FFAs esterification with methanol. The FFAs% conversion determination for these catalysts revealed only a very small amount of FFAs conversion (results not shown). The results demonstrate that SiO_2(x) samples are not active for this reaction.

3.4.1. Cr/SiO_2(x) photocatalysts

Fig. 7 presents the evolution of the FFAs% conversion performed in absence (dark box) and in presence of solar irradiation, as a function of the catalysts calcination temperature. As can be seen, at 35 °C and in the absence of solar irradiation, the FFAs conversions

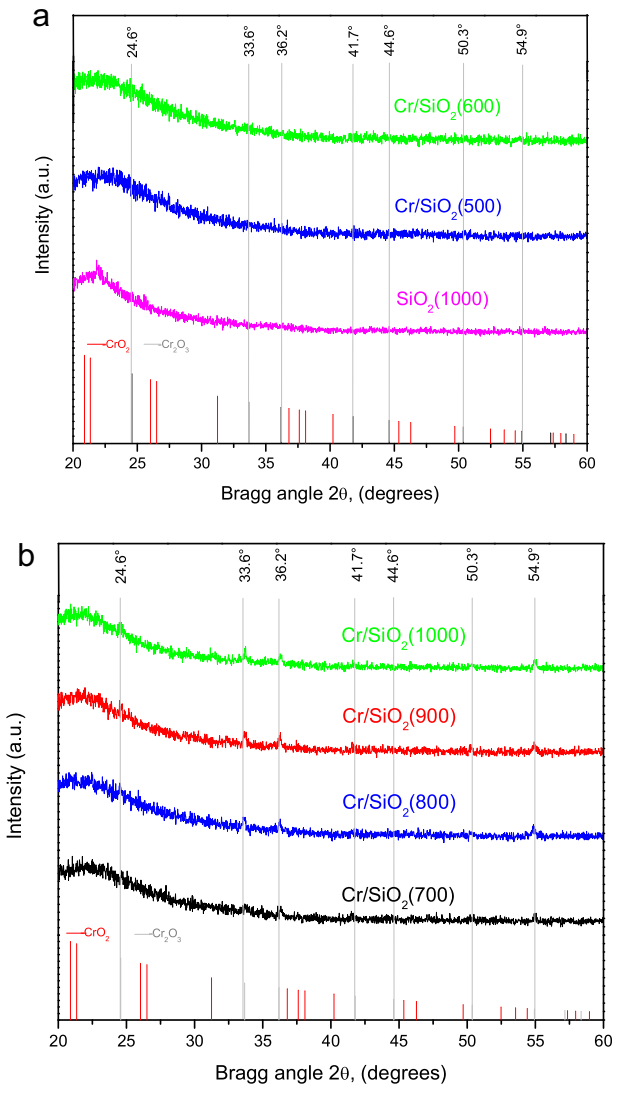

Fig. 6. XRD spectra of (a) $Cr/SiO_2(x)$ photocatalysts (x = 500, 600) and (b) $Cr/SiO_2(x)$ photocatalysts (x = 700, 800, 900, and 1000).

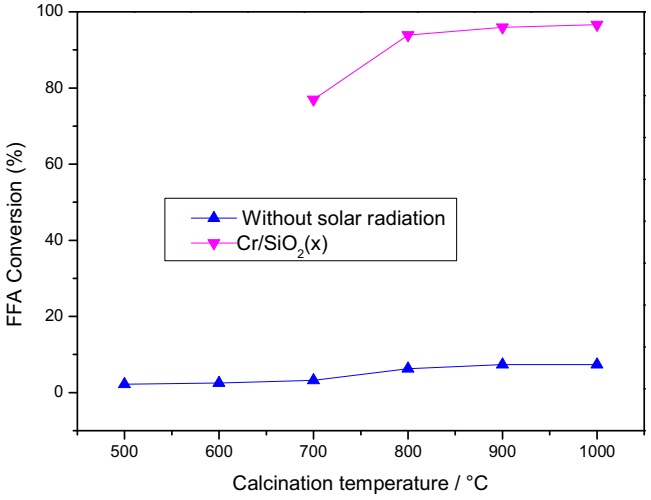

Fig. 7. Effect of solar irradiation on the FFAs% conversion catalyzed by $Cr/SiO_2(x)$ calcined at different temperatures.

by $Cr/SiO_2(x)$ photocatalysts are very low even after 4 h of reaction, indicating that FFAs esterification does not take place over the catalysts at this temperature without solar irradiation.

When the reactor containing the mixture of methanol, WFO and $Cr/SiO_2(500)$, or $Cr/SiO_2(600)$ was placed in the photocatalytic reactor under solar irradiation, an immediate, spontaneous, highly exothermic reaction took place, generating a carbonaceous layer on the catalyst. Under these circumstances, the FFAs photoesterification activity of the catalysts could not be measured. This spontaneous reaction could have been the highly exothermic FFAs and/or methanol adsorption occurring over a large number of acid sites at the catalysts surface ($\sim 10^{19}$ acid sites/g). However, this assumption might not be valid as the same process did not occur when the methanol/WFO was mixed with $Cr/SiO_2(700)$ catalyst, which, as can be seen in Table 3, also presents a very high number of acid sites ($\sim 10^{17}$ acid sites/g).

As the XRD and DRS spectra indicate, the catalysts ($Cr/SiO_2(500)$, and $Cr/SiO_2(600)$) contain a huge amount of Cr^{6+} (with two oxo-bridges). On illumination by solar light, a charge transfer from O^{2-} to Cr^{6+} produces Cr^{5+}-O^{1-} species [26] (Reaction 3) and the reactive oxygen species oxidize adsorbed methanol and/or FFAs, which may undergo a series of consecutive oxidation reactions to produce the highly dehydrogenated carbonaceous molecules detected on the $Cr/SiO_2(500)$, or $Cr/SiO_2(600)$ catalysts (Reaction (4)).

$$Cr^{6+}\text{—}O^{2-} \xrightarrow{h\nu} [Cr^{5+}\text{—}O^{-}]^{*} \quad (3)$$

$$R - COOH, CH_3OH \xrightarrow{[Cr^{5+}\text{—}O^{-}]^{*}} \text{Dehydrogentated carbonaceous molecules} \quad (4)$$

The rate equation (r) for Reaction (4) may depend on the $[Cr^{5+}$-$O^{2-}]$ concentration as given by Eq. (5):

$$r \propto \left[Cr^{5+} - O^{-}\right]. \quad (5)$$

Thus, the reaction rate, which depends directly on the content of Cr^{6+} on the catalyst surface (Reaction (3)), will attain high values in the presence of $Cr/SiO_2(500)$, or $Cr/SiO_2(600)$ catalysts, resulting in the production of dehydrogenated carbonaceous molecules.

On the other hand, when the $Cr/SiO_2(700)$, $Cr/SiO_2(800)$, $Cr/SiO_2(900)$, or $Cr/SiO_2(1000)$ catalysts were placed in the methanol/WFO mixture under solar illumination, the spontaneous exothermic reaction did not take place. As the XRD and DRS spectra and the analysis of the acid sites density revealed, the content of Cr^{3+} species increases in these samples in expense of Cr^{6+} species. The decrease in concentration of Cr^{6+} species in the photocatalysts calcined at higher temperatures lowers the production rate of dehydrogenated carbonaceous molecules.

As can be seen in Fig. 7, for $Cr/SiO_2(700)$, $Cr/SiO_2(800)$, $Cr/SiO_2(900)$, and $Cr/SiO_2(1000)$ catalysts, the FFAs% conversion reaches to very high values at 35 °C under solar irradiation. The high activity of these catalysts can be ascribed to the presence of both Cr^{6+} and Cr^{3+} species in them (Figs. 4 and 5). As the incident solar irradiation covers a wide range of wavelengths, and Cr^{6+} and Cr^{3+} absorb photons of wavelengths between 200 and 500 and 500–700 nm, respectively, both the species may contribute, in a synergetic way, to increase the electron-hole pair generation and to decrease the electron-hole pair recombination rates as described below.

The effect of solar irradiation on FFAs esterification process catalyzed by Cr/SiO_2 can be understood from the schematic energy transfer diagram presented in Fig. 8, showing the generation of electron-hole pairs on Cr^{6+} and Cr^{3+} moieties.

On illumination with solar irradiation of wide spectral range, electron-hole pairs are generated over both the Cr(VI) and Cr(III) oxides in Cr/SiO_2 composite catalysts calcined at or above 700 °C.

Due to the lower band gap energy (~2.3 eV) of CrO_3, the photogenerated electrons will reach to the higher energy states of its conduction band. As the valence band of Cr_2O_3 lies only about 0.25 eV above the conduction band of CrO_3 [27], the free electrons of the conduction band of CrO_3 can easily move to the acceptor levels above the valence band of Cr_2O_3. The holes formed over Cr^{3+} moieties work as traps for the electrons formed over Cr^{6+} moieties, as has been proposed by Zhu et al. [28], Irie et al. [29] and Fan et al. [30] for the observed high activity of Cr^{3+} moieties grafted TiO_2. The filling up of the acceptor levels of Cr_2O_3 would shift its Fermi level upwards, effectively reducing the energy required for generating electron-hole pairs. The later effect would cause the semiconductor (Cr_2O_3) sensitive to the visible light. The occurrence of Fermi level shift and hence visible light sensitivity of Cr_2O_3 while in contact with CrO_3 is supported by the absorption spectra of the composite samples presented in Fig. 4, where we can see an increase in absorption in the visible range and a decrease in the UV range for the catalysts annealed at and beyond 700 °C.

While the electron-hole pairs generated over Cr^{3+} moieties (Cr_2O_3 surface) by the solar light of visible range can also recombine, (following common electron-hole recombination process), a constant supply of free electrons from the conduction band of CrO_3 would keep the valence band and neighboring acceptor level filled. Therefore, there would be a constant production of energetic electrons over Cr^{3+} moieties available for the reduction of FFAs (HOOC-R). On the other hand, the transfer of electrons from the conduction band of CrO_6 would maintain a constant supply of free holes available for the oxidation of CH_3OH over Cr^{6+} moieties. Moreover, the cooperative effect between the Cr^{6+} and Cr^{3+} moieties would increase the concentration of the produced radicals, ($CH_3O\cdot$ and ·HOOC-R), increasing the FFAs esterification rate.

Based on on the proposed mechanism, the FFAs esterification process can take place following the Langmuir-Hinshelwood reaction paths:

1 Transfer of methanol (CH_3OH) and FFA (HOOC-R) to the surface of Cr/SiO(x) photocatalyst. This step may be accelerated by the strong stirring conditions in the reactor.
2 Adsorption of methanol and FFA on the photocatalyst surface, mainly at the Cr^{3+} and Cr^{6+} surface sites which may act as Lewis acid sites. This step may be kinetically favored due to the vast number of acid sites on the catalyst surface.

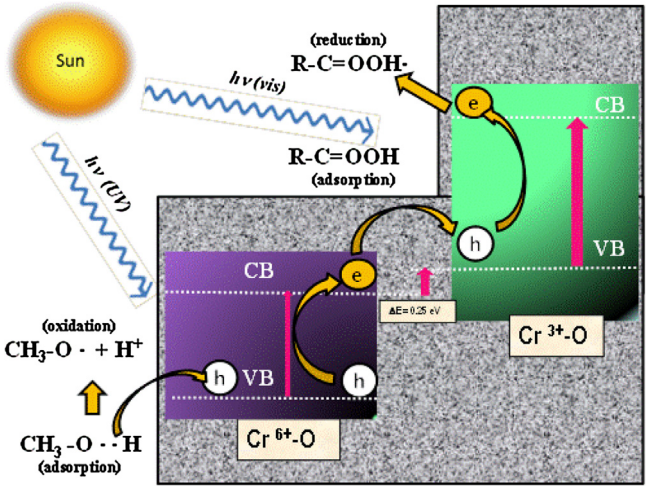

Fig. 8. Schematic presentation of FFAs esterification process over Cr/SiO_2 (800–1000 °C) catalysts under solar irradiation.

3 Photon absorption by Cr/SiO_2 photocatalyst and generation of photo-induced electrons e^- and holes h^+ at Cr^{3+} and Cr^{6+} moieties.
4 The photo-generated holes (h^+) react with CH_3OH adsorbed over the catalyst surface, producing hydrogen ions (H^+) and $CH_3O\cdot$ radicals in a similar way as it has been proposed for the hydrogen production by photocatalytic reforming of methanol [20,21]:

$$CH_3O{\cdot\cdot}H + (h^+) \rightarrow CH_3O\cdot + H^+$$

5 Simultaneously, ·HOOC-R radicals are formed by the reduction of HOOC-R adsorbed over the catalyst surface, reacting with photogenerated electrons (e^-), in a similar way as O_2 reacts with photogenerated e^- to form superoxide species ($\cdot O_2$):

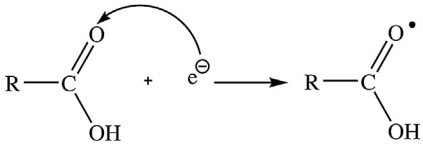

6 Subsequently, the generated H^+, $\cdot O\text{-}CH_3$, and ·HOOC-R react to form the intermediates and final products (methyl-ester and water), as shown in the proposed reaction scheme in Fig. 9.
7 Transfer of the products from the interface region to the liquid phase. This step may be accelerated by the strong stirring conditions in the reactor.

The FFA esterification evolution, photocatalyzed by $1\%Cr/SiO_2$, as a function of the number of runs, at the optimal determined reaction conditions are presented in Fig. 10. As can be seen, even after 10 runs, the activity of the catalyst for FFA photoesterification remains almost unaltered. The results also indicate that the amount of catalyst during the reaction remains unchanged, without a disaggregation of the catalyst in the reaction mixture.

3.5. Alkali catalyzed transesterification of WFO

For the transesterification reaction, the thermal activation required to enhance the interactions between methanol and triglycerides was achieved through direct solar heating. The triglyceride transesterification reactions with methanol were performed under solar irradiation, at 65 °C for 20 min under stirring at 400 rpm.

The transesterification reaction of the triglycerides in WFO after the FFAs photoesterification process (using $Cr/SiO_2(1000)$ catalyst in methanol) was performed with NaOH homogeneous catalyst. Table 5 presents the physical and chemical characteristics of the produced biodiesel. The contents of monoglyceride, diglyceride, triglyceride, free, bound and total glycerin in the final product were determined following the ASTM D 6584 test method. As can be observed, the obtained biodiesel contains very low percentage of these undesired molecules. It is interesting to note (Table 5) a very low value of the chromium concentration in the biodiesel. Utilization of $1\%Cr/SiO_2(1000)$ photocatalyst in FFA esterification generated only 0.0001 wt% of Cr in the produced biodiesel. This result shows that the catalyst preparation was adequate to avoid Cr species leaking during the process. Unchanged catalytic activity of our photocatalysts even after ten FFA photoesterification runs also indicates that there was no catalyst mass loss due to disaggregation and no mass loss of chromium species due to leaching into the reaction mixture.

The fatty acid methyl esters (FAME) composition determined through EN 14103 test method (described in the experimental sec-

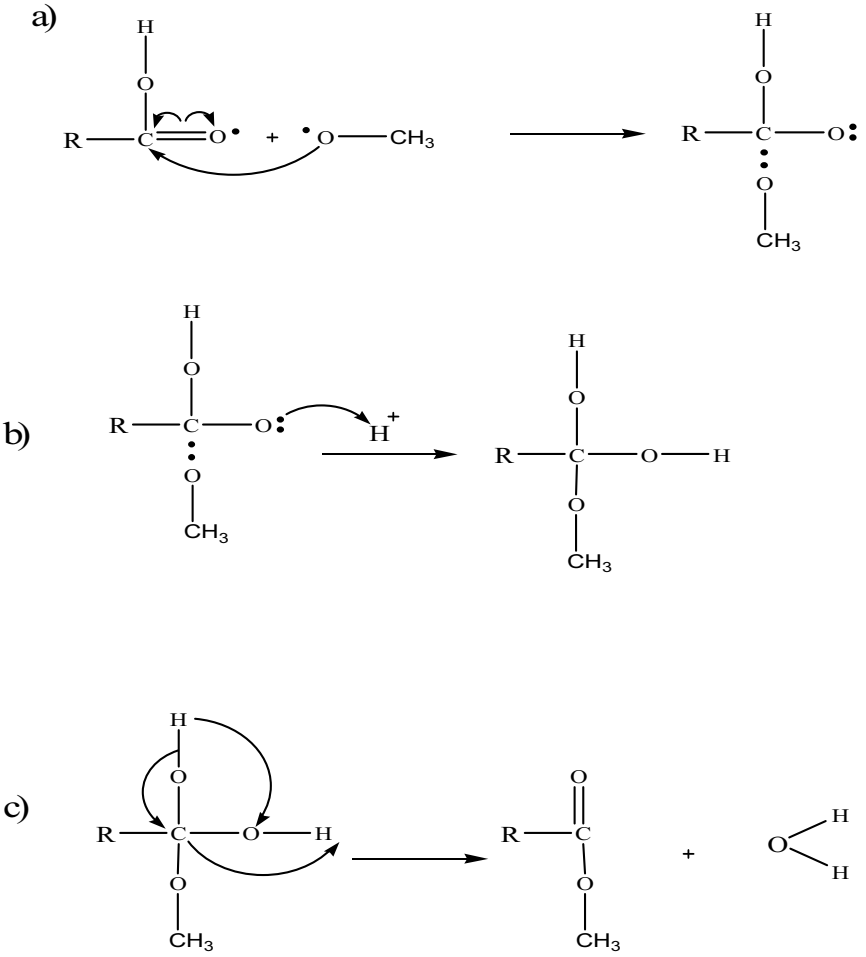

Fig. 9. Reaction scheme for H^+, xO—CH_3, and xHOOC—R interactions leading to the products RCOO—CH_3 and H_2O: (a) the xO—CH_3 radical reacts with the carbonyl group of the xHOOC—R radical, (b) the H^+ reacts with the unstable tetrahedral intermediate, and (c) the tetrahedral intermediate breaks down to fatty acid methyl-ester (RCOO—CH_3) and water.

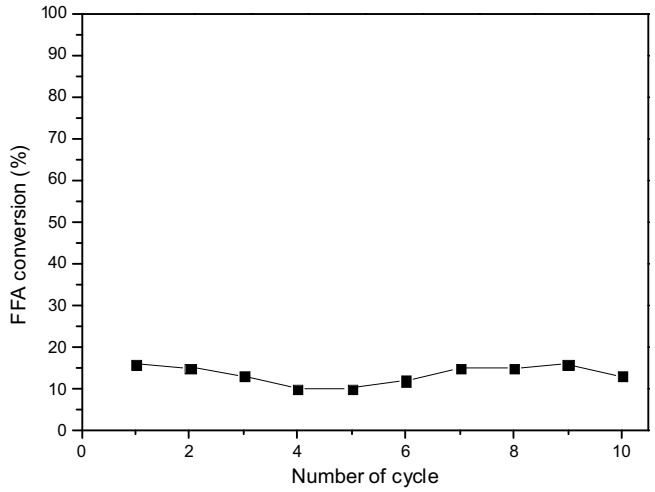

Fig. 10. FFA% conversion as a function of the number of FFA esterification runs over 1% CrO/SiO_2(1000) catalyst.

tion) is reported in Table 6. Very similar values (not presented) were estimated for the produced biodiesel using the WFO esterified by Cr/SiO_2(700), Cr/SiO_2(800) and Cr/SiO_2(900).

The results presented in this work indicate that the photocatalysts Cr/SiO_2(800), Cr/SiO_2(900), and Cr/SiO_2(1000) can generate biodiesel of high purity through esterification of FFAs of WFO, that meets the international quality standard for use and commercialization. The process presented in this study prevents the generation of waste water, use of excess methanol, use of high pressure and costly stainless steel equipment frequently used for the FFAs esterification process of non-edible oils.

A great number of heterogeneous catalysts has been developed to utilize in the production of biodiesel. For example, Ti-incorporated silica [31], calcium oxide [32], MgO [33], $MnCO_3$/ZnO [34] and La/$ZnAl_2O_4$ [35] have been found to be efficient heterogeneous catalysts for this purpose. However, either they are quite expensive, complicate to prepare, or are active only at high temperatures and pressures, which limit their industrial applications. On the other hand, our Cr/SiO_2 photocatalysts are efficient and cheap, active at room temperature and atmospheric pressure, for the process described in this work. On the other hand, they are easy to recover, leading to an inexpensive biofuel production process, thus highly promising for commercial biodiesel production using waste cooking oil as raw material.

4. Conclusions

We have demonstrated the use of Cr/SiO_2 as heterogeneous photocatalyst for efficient esterification of FFAs present in WFO, which is the essential step for the production of biodiesel from non-edible vegetable oils. The Cr/SiO_2 photocatalysts calcined between

Table 5
Characteristics of the biodiesel obtained from WFO using Cr/SiO_2(1000) as photocatalyst for esterification of FFAs, and NaOH as catalyst for transesterification of triglycerides with methanol.

Characteristics /properties	Estimated values	Limiting allowed values
Density at 15 °C	870 kg m^{-3}	(860–900) kg m^{-3}
Kinematic viscosity at 40 °C	3.9 mm^2 s^{-1}	(3.5–5.0) mm^2 s^{-1}
Acid number	0.37 mg KOH g^{-1}	(0.0–0.5) mg KOH g^{-1}
Ester content	96.2 wt%	(96.5–100) wt%
Esters with >4 double bonds	0% wt%	(0.0–1.0) wt%
Esters from linolenic acid (methyl linolenate)	0.01 wt%	(0.0–12.0) wt%
Monoglyceride	0.50 wt%	(0.0–0.8) wt%
Diglyceride	0.15 wt%	(0.0–0.2) wt%
Triglyceride	0.10 wt%	(0.0–0.2) wt%
Free glycerin	0.01 wt%	(0.0–0.02) wt%
Bound glycerin	0.10 wt%	(0.0–0.23) wt%
Total glycerin	0.11 wt%	(0.0–0.25) wt%
Cr species	0.0001 wt%	Not regulated

Table 6
Fatty acid methyl esters (FAME) composition in the biodiesel obtained from WFO using Cr/SiO_2(1000) as photocatalyst for esterification of FFAs, and NaOH as catalyst for transesterification of triglycerides with methanol.

Compound	Content (%)
Methyl butyrate	0.04
Methyl elaidate	65.14
Methyl heptadecanoate	0.08
Methyl hexadecanoate	11.05
Methyl linolaidate	0.08
Methyl decanedioate	3.01
Methyl oleate	10.44
Methyl palmitate	0.45
Methyl palmitoleate	8.02
Methyl pentadecanoate	0.02
Methyl tridecanoate	0.08
Other	1.60
Total	100

700 and 1000 °C manifest very high photocatalytic activity for FFA esterfication under solar irradiation. The high activity of the catalysts is attributed to the co-existence of Cr^{6+} and Cr^{3+} moieties, which can absorb photons of different energy ranges and generate electron-hole pairs at distinct sites. The electrons generated by UV excitation of CrO_3 are transferred to the low-lying acceptor levels of Cr_2O_3, facilitating the generation of electron-hole pairs by visible solar light. Such a cooperative effect between the Cr^{6+} and Cr^{3+} moieties in Cr/SiO_2 composites make them highly effective for photocatalytic esterification of FFAs with methanol. After photoesterification of FFAs, the transesterification reaction of triglycerides present in the WFO could be catalyzed by NaOH to produce high quality biodiesel that meets the international demands for its use and commercialization.

Acknowledgements

The authors acknowledge the financial supports from VIEP, DITCo, BUAP (Grants # VIEP/NAT/49-2016, VIEP/EXC/205-2016, DITCo-2016-5 and DITCo-2016-13) and CONACYT-SENER Cluster Biodiesel Avanzado/250014 extended to perform this research work.

References

[1] S. Palit, A.K. Chowdhuri, B.K. Mandal, Int. J. Glob. Warm. 3 (2011) 232–256.
[2] M. Balat, H. Balat, Appl. Energy 87 (2010) 1815–1835.
[3] A.E. Atabani, A.S. Silitonga, I.A. Badruddin, T.M.I. Mahlia, H.H. Masjuki, S. Mekhilef, Renew. Sustainable Energy Rev. 16 (2012) 2070–2093.
[4] G. Corro, U. Pal, N. Tellez, Appl. Catal. B 129 (2013) 39–47.
[5] Y. Wang, S. Ou, P. Liu, F. Xue, S. Tang, J. Mol. Catal. A 252 (2006) 107–115.
[6] Y.C. Sharma, B. Singh, Fuel 89 (2010) 1470–1474.
[7] Y. Ma, L. Wang, Z. Liu, R. Cheng, L. Zhong, Y. Yang, X. He, Y. Fang, M. Terano, B. Lu, J. Mol. Catal. A 401 (2015) 1–12.
[8] ISO 12937:2000(en). Petroleum products. Determination of wáter. Coulometric Karl Fisher titration method.
[9] Y. Zhang, M.A. Dube, D.D. McLean, M. Kates, Bioresour. Technol. 89 (2003) 1–16.
[10] B.M. Weckhuysen, I.E. Wachs, R.A. Schoonheydt, Chem. Rev. 96 (1996) 3327–3349.
[11] J.S.T. Mambrim, H.O. Pastore, C.U. Davanzo, E.J.S. Vichi, O. Nakamura, H. Vargas, Chem. Mater. 5 (1993) 166.
[12] B.M. Weckhuysen, R.A. Schoonheydt, J.M. Jehng, I.E. Wachs, S.J. Cho, R. Ryoo, S. Kijlstra, E. Poels, J. Chem. Soc. Faraday Trans. 91 (1995) 3245–3253.
[13] B.M. Weckhuysen, R.A. Schoonheydt, F.E. Mabbs, D. Collison, J. Chem. Soc. Faraday Trans. 92 (1996) 2431–2436.
[14] B.W. Weckhuysen, A.A. Verberckmoes, A.R. De Baets, R.A. Schoonheydt, J. Catal. 166 (1997) 160–171.
[15] D. Briggs, M.P. Seah (Eds.), Practical Surface Analysis by Auger and X-Ray Photoelectron Spectroscopy, 2nd ed., Wiley, Chichester, UK, 1990.
[16] B. Liu, Y. Fang, M. Terano, J. Mol. Catal. A 219 (2004) 165–173.
[17] B. Liu, M. Terano, J. Mol. Catal. A 172 (2001) 227.
[18] Y. Fang, B. Liu, M. Terano, Appl. Catal. A 279 (2005) 131–138.
[19] E. Groppo, C. Prestipino, F. Cesano, F. Bonino, S. Bordiga, C. Lamberti, P.C. Thüne, J.W. Niemantsverdriet, A. Zecchina, J. Catal. 230 (2005) 98–108.
[20] L. Liu, H. Li, Y. Zhang, Catal. Today. 115 (2006) 235–241.
[21] A.B. Gaspar, C.A.C. Perez, L.C. Dieguez, Appl. Surf. Sci. 252 (2005) 939–949.
[22] Y.J. Jang, C. Simer, T. Ohm, Mater. Res. Bull. 41 (2006) 67–77.
[23] G. Wu, T. Chen, W. Su, G. Zhou, X. Zong, Z. Lei, C. Li, Int. J. Hydrogen Energy 33 (2008) 1243–1251.
[24] W. Cui, C. Xu, S. Zhang, L. Feng, S. Lü, F. Qiu, J. Photochem. Photobiol. A 175 (2005) 89–93.
[25] J.R. Hwu, C.Y. Hsu, M.L. Jain, Tetrahedron Lett. 45 (2004) 5151–5154.
[26] H. Yamashita, M. Anpo, Curr. Opin. Solid State Mater. Sci. 7 (2003) 471.
[27] M.T. Greiner, M.G. Helander, W.M. Tang, Z.B. Wang, J. Qiu, Z.H. Lu, Nat. Mater. 11 (2012) 76–81.
[28] J. Zhu, Z. Deng, F. Chen, J. Zhang, H. Chen, M. Anpo, J. Huang, L. Zhang, Appl. Catal. B 62 (2006) 329–335.
[29] H. Irie, T. Shibanuma, K. Kamiya, S. Miura, T. Yokoyama, K. Hashimoto, Appl. Catal. B 96 (2010) 142.
[30] X. Fan, X. Chen, S. Zhu, Z. Li, T. Yu, J. Ye, Z. Zou, J. Mol. Catal. A 284 (2008) 155–160.
[31] S.Y. Chen, T. Mochizuki, Y. Abe, M. Toba, Y. Yoshimura, P. Somwongsa, S. Lao-ubol, Appl. Catal. B 181 (2016) 800–809.
[32] A. Demirbas, Energy Convers. Manag. 48 (2007) 937–941.
[33] L.Y. Wang, J.C. Yang, Fuel 86 (2007) 328–333.
[34] L. Wan, H. Liu, D. Skala, Appl. Catal. B 152 (2014) 352–359.
[35] Q.H. Liu, L. Wang, C.X. Wang, W. Qu, Z.J. Tian, H.J. Ma, D. Wang, B.C. Wang, Z.S. Xu, Appl. Catal. B 136 (2013) 210–217.